

# Data-Driven Photoluminescence Tuning in Eu<sup>2+</sup> Doped Phosphors

Shunqi Lai<sup>†</sup>, Ming Zhao<sup>†,‡</sup>, Jianwei Qiao<sup>†,‡</sup>, Maxim S. Molokeev<sup>\*,‡,§</sup>, Zhiguo Xia<sup>\*, †</sup>

<sup>†</sup> State Key Laboratory of Luminescent Materials and Devices, Guangdong Provincial Key Laboratory of Fiber Laser Materials and Applied Techniques, School of Materials Science and Engineering, South China University of Technology, Guangzhou, 510641, China

<sup>#</sup>The Beijing Municipal Key Laboratory of New Energy Materials and Technologies, School of Materials Sciences and Engineering, University of Science and Technology Beijing, Beijing 100083, China

<sup>‡</sup>Laboratory of Crystal Physics, Kirensky Institute of Physics, Federal Research Center KSC SB RAS, Krasnoyarsk 660036, Russia

<sup>Δ</sup>Siberian Federal University, Krasnoyarsk, 660041, Russia

<sup>§</sup>Department of Physics, Far Eastern State Transport University, Khabarovsk, 680021 Russia

---

**ABSTRACT:** The design of new phosphors has long relied on the chemical intuition and time-intensive trial-and-error experimental synthesis, therefore searching new materials assisted by data-driven computations through artificial intelligence (AI) is critical. Herein, we utilize a regression model to predict the emission wavelengths of Eu<sup>2+</sup> doped phosphors by revealing the relationship between the crystal structure and luminescence properties. The emission wavelengths of [Rb<sub>(1-x)</sub>K<sub>(x)</sub>]<sub>3</sub>LuSi<sub>2</sub>O<sub>7</sub>:Eu<sup>2+</sup> (0 ≤ x ≤ 1) phosphors, as examples for the data-driven photoluminescence tuning, are successfully predicted based on the existed data of eight systems, also consistent with the experimental results. These phosphors can be excited by blue light and exhibit broad-band red and near-infrared emission ranging from 619 to 737 nm. These findings in Eu<sup>2+</sup> doped silicate phosphors indicate that data-driven computations through AI would have bright application foreground in discovering novel phosphors with a target emission wavelength.

---

## ■ INTRODUCTION

Phosphor-converted light-emitting diodes (*pc*-LEDs) have become the next-generation lighting source due to high efficiency, low energy consumption, long lifetime, and environmental compatibility.<sup>1-3</sup> Until now, *pc*-LEDs technology has been widely used in many fields, such as general lighting, automotive lighting, display backlight, medical diagnostics, plant lighting, and so on.<sup>4-7</sup> Therefore, it is critical to develop phosphors with appropriate emission wavelengths, and many strategies have been adopted to discover new phosphors, such as trial-and-error searching in crystal structure databases, combinatorial chemistry screening with high throughput experimentation, chemical unit co-substitution based on a structural model, or single-particle diagnosis approach.<sup>8,9</sup> Thus, many novel phosphors with various emission wavelengths have been discovered through those approaches.<sup>10-12</sup> Nevertheless, these methods are largely conducted through painstaking experiments in an Edisonian fashion, which require the abundant experience and massive experimentation.<sup>9</sup> Driven by the rapid development of computers, the advancement of algorithms, and the explosion of experimental material databases, machine learning techniques have become powerful tools for materials discovery.<sup>13,14</sup> Recently, data-driven methodologies have been used in computational design and experimental identification for novel phosphors. Brgoch's group established a thermally robust phosphor NaBaB<sub>9</sub>O<sub>15</sub>:Eu<sup>2+</sup> with the assistance of machine learning and high-throughput density functional theory (DFT) calculations.<sup>15</sup> In addition, Wang et al. adopted a carefully targeted data-driven structure pre-

diction and screening effort to discover a new phosphor, Sr<sub>2</sub>LiAlO<sub>4</sub>, the first known Sr-Li-Al-O quaternary crystal.<sup>16</sup> Data-driven methodologies provide a convenient way to find novel phosphors, however, the core problem is to propose decision rules, which enable us to establish a mapping between measurable and easily accessible attributes of a system and its properties.<sup>17</sup>

The relationship between crystal structure and luminescence properties is always a holy grail for the phosphor materials discovery.<sup>18,19</sup> Nevertheless, structure-property association study is a challenge owing to the multiparameter and complexity of the task. *Ab initio* theoretical calculations can predict the structure-property relationship, but it has a heavy workload on account of the huge calculations and the special knowledge needs. Artificial intelligence (AI) can make easily predictions if there is an adequate database. Amongst, machine learning acting as a hot tool, usually demands more examples, in contrast to the limited amounts of phosphor materials with particular interests. However, regression analysis, as another way, refers to a set of statistical processes for estimating the relationships between a dependent variable, called the 'outcome variable', and one or more independent variables, also called 'predictors', 'covariates', or 'features'.<sup>20</sup> This analysis is not so restricted to the amounts of samples and can be easily applied to database of 10-100 samples. There are many types of regression analysis, including simple regression, multiple regression, logistic regression and so on.<sup>21</sup> For instance, Pilania et al. successfully used a kernel ridge regression model to predict the electronic properties.<sup>17</sup> Here, we use simple regression analysis to

establish the relationship of crystal structure and luminescence properties to predict the emission wavelength of the unknown phosphors.

Previously, we discovered a series of  $\text{Eu}^{2+}$  doped  $\text{A}_3\text{BSi}_2\text{O}_7$ -type (A = alkali metal ions; B = rare-earth metal ions) phosphors, such as  $\text{K}_3\text{YSi}_2\text{O}_7:\text{Eu}^{2+}$ ,  $\text{K}_3\text{LuSi}_2\text{O}_7:\text{Eu}^{2+}$ ,  $\text{Rb}_3\text{YSi}_2\text{O}_7:\text{Eu}^{2+}$ ,<sup>22-24</sup> which can be excited by blue light and emit red or near-infrared light. The typical  $\text{A}_3\text{BSi}_2\text{O}_7$  compounds have similar structures and the local structure only can be affected by the A and B ions. Hence, two parameters of ion radius A and B need to be varied during the process of modeling, which greatly reduces the modeling difficulty. In this work, the luminescence properties of some reported phosphors in  $\text{A}_3\text{BSi}_2\text{O}_7:\text{Eu}^{2+}$  families are chosen as the database, and regression analysis is used to establish a model that can predict the emission wavelengths of the class of phosphors. The solid solution phosphors formed by  $\text{K}_3\text{LuSi}_2\text{O}_7:\text{Eu}^{2+}$  and  $\text{Rb}_3\text{LuSi}_2\text{O}_7:\text{Eu}^{2+}$  are chosen to verify the accuracy of the model. The photoluminescence tuning of  $[\text{Rb}_{(1-x)}\text{K}_{(x)}]_3\text{LuSi}_2\text{O}_7:\text{Eu}^{2+}$  ( $0 \leq x \leq 1$ ) (abbreviated as  $\text{R}_{1-x}\text{K}_x\text{LSO}:\text{Eu}^{2+}$ ) is accordant with the results predicted by simple regression analysis. In addition, all the phosphors exhibit broad red to near-infrared emission band under blue light excitation, which can be applied to the new lighting source. The results suggest that simple regression analysis is potentially a good method to predict the emission wavelength of unknown phosphors.

## ■ EXPERIMENTAL SECTION

**Sample Preparation.**  $\text{R}_{1-x}\text{K}_x\text{LSO}:0.01\text{Eu}^{2+}$  ( $0 \leq x \leq 1$ ) powders were synthesized via high-temperature solid-state reaction. The stoichiometric mixtures of  $\text{K}_2\text{CO}_3$  (A.R.),  $\text{Rb}_2\text{CO}_3$  (A.R.),  $\text{Lu}_2\text{O}_3$  (99.99%),  $\text{SiO}_2$  (A.R.), and  $\text{Eu}_2\text{O}_3$  (99.99%) were thoroughly grounded and transferred into an alumina crucible. After that, the mixed starting materials were sintered at 1000 - 1200 °C for 6 h under a reducing atmosphere ( $\text{N}_2 : \text{H}_2 = 80\% : 20\%$ ) in a tube furnace. After the calcinations, the samples were slowly cooled to room temperature and crushed into powders for further characterization.

**Characterization.** The phase and purity of the as-prepared powder samples were examined by X-ray diffraction (XRD) analysis using an Aeris powder diffractometer (PANalytical Corporation, Netherlands) operating at 40 kV and 15 mA with monochromatized Cu K $\alpha$  radiation ( $\lambda = 1.5406 \text{ \AA}$ ). Rietveld refinement was conducted using TOPAS 4.2 software. Photoluminescence (PL) and Photoluminescence excitation (PLE) spectra

were measured by an Edinburgh FLS920 fluorescence spectrometer equipped with continuous xenon (Xe) lamps (450 W). The fluorescent decay curves were also measured by the FLS920 instrument with an nF900 flash lamp as the excitation source.

## ■ RESULTS AND DISCUSSION

To construct the general prediction model, one should have information on two numeric characteristics for each member of a group, which are related to each other. In such a situation, it is able to plot the data related to the characteristics of a scatter diagram. If the dots fall roughly along a straight line, sloping either upwards or downwards, it will conclude that a relationship exists. As a next step, linear regression analysis is used to make the relationship computable, which means that knowing the value of one variable can predict the value of the other variable in the group. The known value variable refers to the independent variable, and the predicted variable refers to the dependent variable. The independent and dependent variables, by convention, refer to “ $x$ ” and “ $y$ ”, plotting as horizontal and vertical axes, respectively. Namely, linear regression analysis on two variables ( $x$  and  $y$ ) in a sample can be looked upon as plotting the data to a best-fit line as is shown in Figure 1a. This best fit line is chosen in the minimum sum of squares of all the residuals (the vertical distance of each point from the line), as least-squares line. This line can be mathematically defined by an equation of the form:

$$Y = a + bx \quad (1)$$

where “ $x$ ” is the known value of the independent variable, “ $Y$ ” is the predicted value of “ $y$ ” for the given value of “ $x$ ”, “ $a$ ” is called as the “intercept” of the estimated line, representing the value of  $Y$  when  $x = 0$ , and “ $b$ ” is called as the “slope” of the estimated line representing the amount by which  $Y$  changes on average as “ $x$ ” increases by one unit. It is also referred to “coefficient”, “regression coefficient”, or “gradient”.<sup>19,20</sup>

**Table 1.** Excitation and emission wavelengths of  $\text{A}_3\text{BSi}_2\text{O}_7:\text{Eu}^{2+}$  phosphors obtained by experiments.

Materials	Excitation, nm	Emission, nm
$\text{K}_3\text{LaSi}_2\text{O}_7$	365	530
$\text{K}_3\text{YSi}_2\text{O}_7$	450	620 <sup>22</sup>
$\text{K}_3\text{GdSi}_2\text{O}_7$	400	630
$\text{K}_3\text{LuSi}_2\text{O}_7$	450	740 <sup>24</sup>
$\text{K}_3\text{ScSi}_2\text{O}_7$	450	740
$\text{Rb}_3\text{YSi}_2\text{O}_7$	450	622 <sup>23</sup>
$\text{Rb}_3\text{GdSi}_2\text{O}_7$	330	550
$\text{Rb}_3\text{LuSi}_2\text{O}_7$	450	619

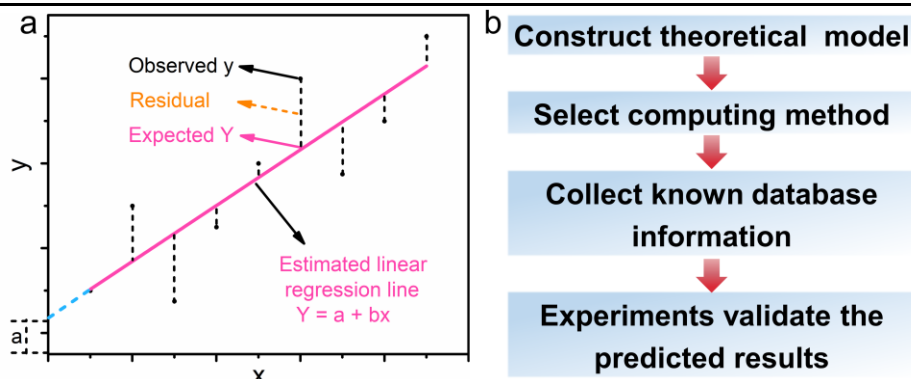


**Figure 1.** (a) Data from a sample and the estimated linear regression line for these data. Each dot corresponds to a data point, i.e., an individual pair of values for  $x$  and  $y$ , and the vertical dashed lines from each dot represent residuals. The capital letters ( $Y$ ) are used to indicate predicted values and lowercase letters ( $x$  and  $y$ ) for known values. Intercept is shown as “ $a$ ” and slope or regression coefficient as “ $b$ ”. (b) The full data-driven steps for predicting.

As a summary, the data-driven steps for prediction are shown in Figure 1b. Here, we use linear regression analysis to establish the relationship of structure and luminescence properties to predict the emission wavelength of a class of phosphors  $A_3BSi_2O_7:Eu^{2+}$ . There are only two varied parameters, ion radii of A ( $\text{\AA}$ ) and B ( $\text{\AA}$ ) for the  $A_3BSi_2O_7:Eu^{2+}$  phosphors, where ion radii A and B refer to  $x$ , and  $y$  refers to the emission wavelength, as demonstrated by the crystal structure model and emission spectra of  $A_3BSi_2O_7:Eu^{2+}$  phosphors (Figure 2a and 2b). Due to those, we obtain a linear function of ion radii:

$$W_e = a \times IR(A) + b \times IR(B) + c \quad (2)$$

where  $W_e$  refer to the emission wavelength, and  $a$ ,  $b$ ,  $c$  refer to some unknown constants which should be defined (Figure 2c). We used the information about the wavelength emission of several known  $A_3BSi_2O_7:Eu^{2+}$  phosphors (Table 1) to make fitting. The excitation wavelength varies from 330 to 450 nm, but we did not focus on it and it is found a small effect of excitation on emission at the first stage. After regression analysis, the equation appeared to be:

$$W_e = 2364.586 - 644.061 \times IR(A) - 775.554 \times IR(B) \quad (3)$$

Therefore, the equation (3) was used to predict the emission of  $[Rb_{(1-x)}K_x]_3LuSi_2O_7:Eu^{2+}$  and theoretically

predicted and experimentally observed emission wavelengths are depicted in Figure 2d. The residual between expected and all observed data was in the range of 5-50 nm, and maximum value seems to be not very good. However, one can see that the trend in Figure 2d was revealed very well, and similar trends can be also obtained for any compound with chemical formula of  $A_3BSi_2O_7:Eu^{2+}$ , and it opens many possibilities. Moreover, the analysis of the equation (3) revealed that: 1) The increasing of A and B ion radii should lead to a blue shift of wavelength emission. For example, most Cs-containing or La-containing compounds should lead to blue shift; 2) By contrary, the decreasing of the radii of A and B ions should lead to redshift. For example, Na-containing or Lu-containing compounds should lead to redshift; 3) A ion has a bigger influence on wavelength than B ion, because usually ion radii A vary in the range of 1.24-1.78  $\text{\AA}$  (Na-Cs ions), but B ions vary in the more narrow range 1.032-1.216  $\text{\AA}$  (Lu-La ions) and the absolute value is smaller, but coefficients of  $a = -644.061$  and  $b = -775.554$  are similar. Thus, the simple formula with only three variables revealed the global trends, structure-property relationships, which are very important in material sciences.

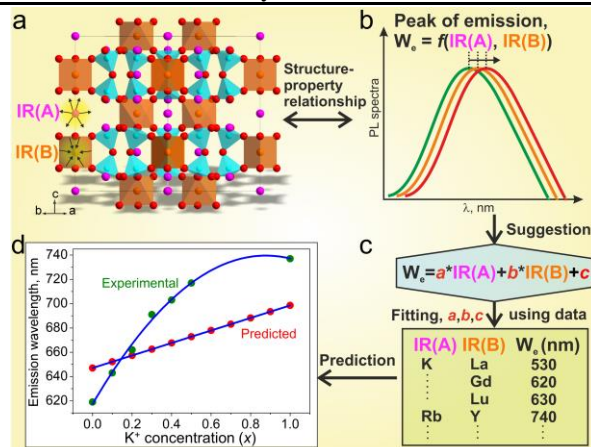


**Figure 2.** (a-b) The crystal structure model of  $A_3BSi_2O_7$ , and the relationship between structure and luminescence property. (c) The assumed formula and the related database for prediction. (d) Theoretically predicted and experimentally observed emission wavelengths of  $R_{1-x}K_xLSO:0.01Eu^{2+}$  ( $0 \leq x \leq 1$ ) phosphors.

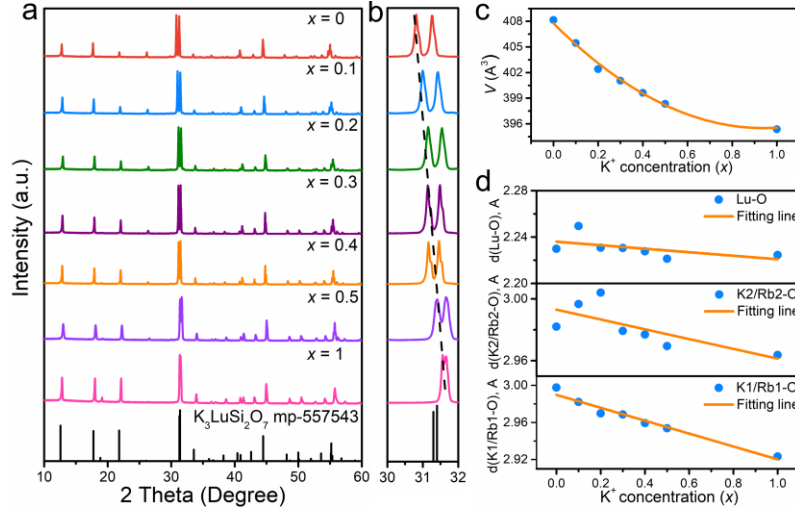


**Figure 3.** (a) The standard pattern (obtained from Materials Project, mp-557543) of  $K_3LuSi_2O_7$  and as-measured XRD patterns of  $R_{1-x}K_xLSO:0.01Eu^{2+}$  ( $0 \leq x \leq 1$ ). (b) The selected diffraction peaks near  $31^\circ$  of  $R_{1-x}K_xLSO:0.01Eu^{2+}$  ( $0 \leq x \leq 1$ ). (c) Cell volume  $V(x)$  dependence of  $K^+$  concentration. (d) Dependence of the average bond length of Lu, K1/Rb1, and K2/Rb2 in  $R_{1-x}K_xLSO:0.01Eu^{2+}$  ( $0 \leq x \leq 1$ ).

To further check the rationality of the data-driven photoluminescence tuning revealed by the regression model and explain the possible mechanisms, the phase structures and luminescence properties of  $R_{1-x}K_xLSO:0.01Eu^{2+}$  phosphors have been investigated in detail. Figure 3a shows the XRD patterns of the as-prepared  $R_{1-x}K_xLSO:0.01Eu^{2+}$  solid solution, which can be well indexed to the reported pattern of a hexagonal ( $P6_3/mmc$ ) phase  $K_3LuSi_2O_7$ . Due to the smaller ionic radius of  $K^+$  ion than  $Rb^+$  ion, the enlarged diffraction peaks from  $2\theta = 30^\circ - 32^\circ$  of  $R_{1-x}K_xLSO:0.01Eu^{2+}$  samples continuously shift toward larger angles with the increase of  $x$  compared with the position of  $Rb_3LuSi_2O_7:0.01Eu^{2+}$  (Figure 3b), indicating there is a lattice shrinkage with substituting  $Rb^+$  by  $K^+$ . Moreover, further Rietveld refinement of the series of  $R_{1-x}K_xLSO:0.01Eu^{2+}$  have been performed, and the main parameters are shown in Table S1.  $K_3LuSi_2O_7$  was taken as the starting model for Rietveld refinement.<sup>25</sup> The sites of  $K^+$  ions are occupied by  $K^+/Rb^+$  ions according to the suggested chemical formula. Minor impurity phases of  $Lu_2O_3$  were found at about 0.8~1.5%, which would have no impact on the luminescence properties of these phosphors. Furthermore, the variations of the cell volumes and bond lengths of each sample are shown in Figure 3c-d, and coordinates of atoms and main bond lengths are shown in Tables S2 and S3, respectively. Obviously, the relative content of K and Rb has little effect on the average bond lengths of Lu-O, while the average bond lengths of K1/Rb1-O and K2/Rb2-O decrease almost linear as the increase of  $K^+$  concentration, which indicates  $K^+$  ions have definitely entered the  $Rb^+$  lattice to form a solid solution. It is further confirmed by the cell volume ( $V$ ) of  $R_{1-x}K_xLSO:0.01Eu^{2+}$  samples, which decreases linearly with  $x$  in good agreement with the fact that the  $K^+$  ion has a smaller ionic radius than the  $Rb^+$  ion obeying the Vegard's rule.<sup>26</sup>

The crystal structures of  $Rb_3LuSi_2O_7$  display a similar atom configuration with that of  $K_3LuSi_2O_7$ . As seen in Figure 2a, all the fundamental frameworks are constructed by  $LuO_6$  octahedra and  $Si_2O_7$  units via vertex-sharing.  $K^+/Rb^+$  displays the same coordination form in the channel composed by  $LuO_6$  octahedra and  $Si_2O_7$  units, which sites with 9-fold ( $K1/Rb1$ ) and 6-fold ( $K2/Rb2$ ) coordination in the unit cell and form two kinds of polyhedrons connected with each other by sharing the same vertexes and edges. In  $K_3LuSi_2O_7$ , the main doping mechanism is ascribed to the synergetic effect of  $Lu \rightarrow Eu$  and  $K2 \rightarrow Eu$  replacements, as discussed before.<sup>22-24</sup> Due to the similar crystal structure and the same cationic coordination environment in  $R_{1-x}K_xLSO:Eu^{2+}$  samples, the main doping mechanism of Eu ion remains unchanged, which is further illustrated in the following analysis of luminescence performance. This same crystal structure and  $Eu^{2+}$  occupancy in  $A_3BSi_2O_7:Eu^{2+}$  phosphors guarantees the results obtained from the regression model.

As shown in Figure 4a, the PLE spectra of  $R_{1-x}K_xLSO:0.01Eu^{2+}$  samples possess broad-band excitation in the region of 250 nm - 600 nm and these phosphors are suitable for the commercial blue chips. The excitation peaks position and shape are almost unchanged with increasing substituted cation concentration in  $R_{1-x}K_xLSO:0.01Eu^{2+}$  samples, except for slightly increasing of bandwidth. Upon 450 nm excitation, the PL spectra of  $R_{1-x}K_xLSO:0.01Eu^{2+}$  exhibit a consecutive redshift from orange-red light to near infrared light with the increase of  $K^+$  concentration as shown in Figure 4b. As is shown in Table S4, it displays that the emission peak shifts from 619 nm to 737 nm. Moreover, all PL spectra can be decomposed into two Gaussian curves, which indicates that  $Eu^{2+}$  ions occupy two different sites, as shown in Figure 4c. Photoluminescence decay lifetime is an efficient

method to analyze the sites occupation in phosphor materials. All the photoluminescence decay curves of  $[K^+ \rightarrow Rb^+]$  phosphors obey the bi-exponential model (Figure S1), which further certifies that  $Eu^{2+}$  occupies two cation

sites (K2/Rb2 and Lu sites), as discussed before. The calculated lifetime values changed gradually, which is related to the energy transfer among two  $Eu^{2+}$  centers.

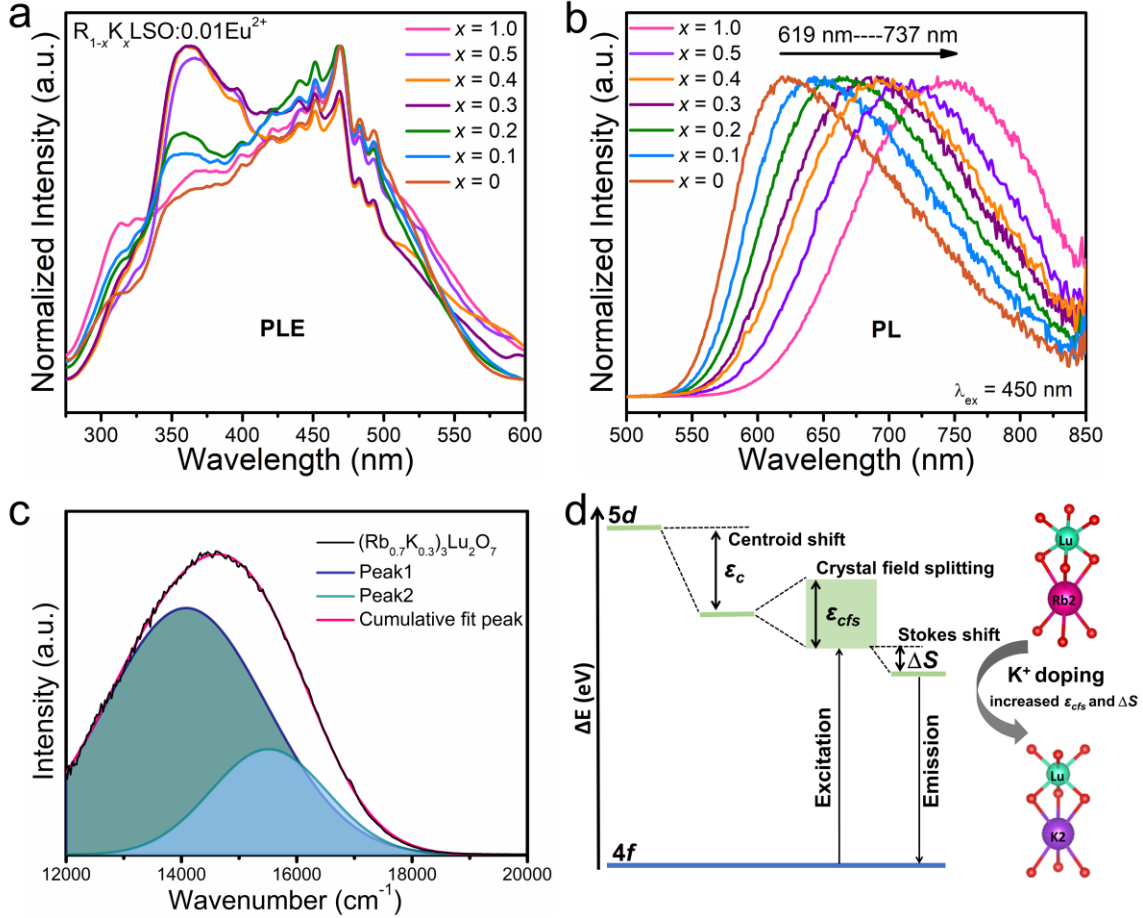


**Figure 4.** (a) Normalized PLE and (b) PL spectra of as-prepared  $R_{1-x}K_xLSO:0.01Eu^{2+}$  ( $0 \leq x \leq 1$ ). (c) The Gaussian fitting curves of the  $R_{1-x}K_xLSO:0.01Eu^{2+}$  ( $x = 0.3$ ). (d) The schematic mechanism diagram of the tunable spectra in  $R_{1-x}K_xLSO:0.01Eu^{2+}$  ( $0 \leq x \leq 1$ ) phosphors.  $\epsilon_c$  denotes the centroid shift of  $5d$ -levels of  $Eu^{2+}$ ,  $\epsilon_{cfs}$  shows the crystal field splitting effect and  $\Delta S$  refers to the Stokes shift.

To better understand the large-scale emission tuning in  $R_{1-x}K_xLSO:0.01Eu^{2+}$  phosphors, the local lattice environment around  $Eu^{2+}$  is used to reveal the intrinsic mechanism. For  $R_{1-x}K_xLSO:0.01Eu^{2+}$  phosphor, the centroid shift has a weak effect on the redshift because of the low covalence between  $Eu^{2+}$  and  $O^{2-}$  ions. Considering the sensitivity of  $Eu^{2+}$  ions to the crystal field environment, the cation substitution of  $K^+$  for  $Rb^+$  would directly influence the luminescence properties. When  $Rb^+$  ions are substituted by  $K^+$  ions, the  $K^+$  ions randomly occupy the  $Rb^+$  sites, including the neighboring  $Rb^+$  sites around the  $Eu^{2+}$  ions. The local structural variation caused by cation substitution around the luminescent centers would definitely influence the crystal field strength.<sup>24</sup> On the basis of crystal field theory, the type of polyhedron and bond length between the central cation and its ligands are important factors in determining the crystal field strength of the  $Rb^+$  sites occupied by  $K^+$  ions. In general, the crystal field strength ( $D_q$ ) could be identified via the expression:<sup>27</sup>

$$D_q = \frac{Ze^2r^4}{6R^5} \quad (4)$$

where  $Z$  is the charge or valence of the anion,  $e$  is the electron charge,  $r$  refers to the radius of the  $d$  wavefunction, and  $R$  is the bond length between the central cation and its ligands. The  $D_q$  value is inversely proportional to  $R$  value. Theoretically, the substitution of  $Rb^+$  by  $K^+$  would generate an increased crystal field splitting due to the decreased  $R$  value, which reduces the energy of lowest  $5d$  level. The emission spectrum is determined by the lowest  $5d$  energy level and Stokes shift. Herein, we further estimated the Stokes shift from Figure 4a-b, which is twice the energy difference between the intersection point of excitation and emission spectra and the peak of the emission spectra.<sup>28,29</sup> It increases from  $3586 \text{ cm}^{-1}$  to  $5152 \text{ cm}^{-1}$  with the increasing of  $K^+$  concentration. Since the Stokes shift is greatly influenced by the rigidity of crystal structure, the substitution of  $K^+$  ions could impair the rigidity, leading to the gradually increasing Stokes

shift, which results in the spectral redshift.<sup>30,31</sup> Therefore, we can reasonably conclude that the redshift is caused by the combined effect of Stokes shift and crystal field strength. The schematic energy level diagram for Eu<sup>2+</sup> ions in RKL<sub>x</sub>SO:0.01Eu<sup>2+</sup> phosphors is shown in Figure 4d.

When we recall the comparison between the maximum emission wavelengths of the experiment and the prediction depicted in Figure 2d, one can find that the increasing trend is almost the same as predicted by the simple regression analysis. These results suggest that it is a potentially good way to predict the emission wavelength of unknown phosphors. It is interesting that the simple model and easy calculations could give us predictive conclusions. More complex compounds not only for the solid solution but also the isostructural compounds can be also treated by using this model. With abundant data, the predictions would be more accurate. Therefore, experimentally investigating this series of phosphors will provide much support to the regression analysis as a tool for identifying the emission wavelength of new inorganic phosphors.

## ■ CONCLUSIONS

In summary, the construction of a calculation model based on the connection between crystal structure and luminescence properties in A<sub>3</sub>BSi<sub>2</sub>O<sub>7</sub>:Eu<sup>2+</sup> (A = alkali metal ions; B = rare-earth metal ions) is used to identify the emission wavelength of unknown inorganic phosphors. With the assistance of simple regression analysis, the increasing/decreasing of A and B ion radii should lead to a blue/red shift of wavelength emission and A ion has a bigger influence on wavelength than B ion. We established a linear function of ion radii to predict the emission wavelengths of R<sub>1-x</sub>K<sub>x</sub>LSO:0.01Eu<sup>2+</sup> phosphors, and the emission peaks displays the shifts from 619 nm to 737 nm with the *x* increasing from 0 to 1. The redshift of emission spectra is attributed to the combined effect of the increased crystal field splitting and the increased Stokes shift. These results support that regression analysis is an indispensable method to direct the search for new rare-earth phosphors even if the amount of samples is very small and not appropriate for machine learning. All the phosphors show the red emission under the excitation of blue light, indicating they have potential applications in new lighting source, and the methods used have a good directivity for the future application of regression analysis for other functional materials.

## ASSOCIATED CONTENT

### Supporting Information

The Supporting Information is available free of charge on the ACS Publications website at DOI:

The photoluminescence decay curves of R<sub>1-x</sub>K<sub>x</sub>LSO:0.01Eu<sup>2+</sup> for Figure S1; main parameters of re-

finement, coordinates of atoms, main bond lengths and specific emission wavelength of the mentioned samples for Table S1-S4 (PDF).

## AUTHOR INFORMATION

### Corresponding Author

\*E-mail: [xiazg@scut.edu.cn](mailto:xiazg@scut.edu.cn)

### Notes

The authors declare no competing financial interest.

## ACKNOWLEDGMENTS

The present work was supported by the National Natural Science Foundations of China (Grant No. 51972118, 51961145101 and 51722202), Fundamental Research Funds for the Central Universities (D2190980), the Guangdong Provincial Science & Technology Project (No. 2018A050506004), and the Local Innovative and Research Teams Project of Guangdong Pearl River Talents Program (2017BT01X137). This work is also funded by RFBR according to the research project No. 19-52-80003.

## REFERENCES

- (1) Reineke, S., Complementary LED Technologies. *Nature Mater.* **2015**, 14, 459-462.
- (2) Xia, Z.; Xu, Z.; Chen, M.; Liu, Q., Recent Developments in the New Inorganic Solid-State LED Phosphors. *Dalton T.* **2016**, 45, 11214-11232.
- (3) Wei, Y.; Yang, H.; Gao, Z.; Liu, Y.; Xing, G.; Dang, P.; Abdulaziz A. Al Kheraif.; Li, G.; Lin, J.; Liu, R., Strategies for Designing Antithermal-Quenching Red Phosphors. *Adv. Science.* **2019**, 1902060.
- (4) Zhao, M.; Liao, H.; Molokeev, M.S.; Zhou, Y.; Zhang, Q.; Liu, Q.; Xia, Z., Emerging Ultra-Narrow Band Cyan-Emitting Phosphor for White LEDs with Enhanced Color Rendition. *Light, sci. appl.* **2019**, 8, 38.
- (5) Hoppe, H.; Recent Developments in the Field of Inorganic Phosphors. *Angew. Chem.* **2009**, 48, 3572-82.
- (6) Tang, Z.; Zhang, Q.; Cao, Y.; Li, Y.; Wang, Y., Eu<sup>2+</sup>-Doped Ultra-Broadband VIS-NIR Emitting Phosphor. *Chem. E. J.* **2020**, 388, 124231.
- (7) Mao, Z.; Li, J.; Wang, D., Dual-Responsive Sr<sub>2</sub>SiO<sub>4</sub>:Eu<sup>2+</sup>-Ba<sub>3</sub>MgSi<sub>2</sub>O<sub>8</sub>:Eu<sup>2+</sup>, Mn<sup>2+</sup> Composite Phosphor to Human Eyes and Plant Chlorophylls Applications for General Lighting and Plant Lighting. *Chem. E. J.* **2016**, 284, 1003-1007.
- (8) Xia, Z.; Liu, Q., Progress in Discovery and Structural Design of Color Conversion Phosphors for LEDs. *Pro. Mater. Sci.* **2016**, 84, 59-117.
- (9) Li, S.; Xie, R., Critical Review—Data-Driven Discovery of Novel Phosphors. *ECS J. Solid State Sci. Technol.* **2019**, 9, 016013.
- (10) Qiao, J.; Zhao, J.; Xia, Z., A Review on the Eu<sup>2+</sup> Doped β-Ca<sub>3</sub>(PO<sub>4</sub>)<sub>2</sub>-Type Phosphors and the Sites Occupancy for Photoluminescence Tuning. *Opt. Mater.: X.* **2019**, 1, 100019.
- (11) Cheng, C.; Ning, L.; Ke, X.; Molokeev, M.S.; Wang, Z.; Zhou, G.; Chuang, Y.; Xia, Z., Designing High-Performance LED Phosphors by Controlling the Phase Sta-

bility via a Heterovalent Substitution Strategy. *Adv. Opt. Mater.* **2019**, 8, 1901608.

(12) Takeda, T.; Hirosaki, N.; Funahshi, S.; Xie, R., Narrow-Band Green-Emitting Phosphor  $\text{Ba}_2\text{LiSi}_7\text{AlN}_{12}:\text{Eu}^{2+}$  with High Thermal Stability Discovered by a Single Particle Diagnosis Approach. *Chem. Mater.* **2015**, 27, 5892-5898.

(13) Zhuo, Y.; Hariyani, S.; Armijo, E.; Abolade Lawson, Z.; Brgoch, J., Evaluating Thermal Quenching Temperature in  $\text{Eu}^{3+}$ -Substituted Oxide Phosphors via Machine Learning. *ACS Appl. Mater. Interfaces.* **2020**, 12, 5244-5250.

(14) Butler, K.; Davies, D.; Cartwright, H.; Isayev, O.; Walsh, A., Machine Learning for Molecular and Materials Science. *Nature.* **2018**, 559, 547-555.

(15) Zhuo, Y.; Mansouri Tehrani, A.; Oliynyk, A.O.; Duke, A.C.; Brgoch, J., Identifying an Efficient, Thermally Robust Inorganic Phosphor Host via Machine Learning. *Nat. Commun.* **2018**, 9, 4377.

(16) Wang, Z.; Ha, J.; Kim, Y.H.; Im, W.; McKittrick, J.; Ong, S., Mining Unexplored Chemistries for Phosphors for High-Color-Quality White-Light-Emitting Diodes. *Joule.* **2018**, 2, 914-926.

(17) Pilia, G.; Wang, C.; Jiang, X.; Rajasekaran, S.; Ramprasad, R., Accelerating Materials Property Predictions Using Machine Learning. *Sci. Rep.* **2013**, 3, 2810.

(18) Ding, X.; Cao, H.; Mu, Y.; Zhu, G.; Xia, D., The Structure and Photoluminescence Properties of A Novel Orange Emission Phosphor  $\text{Ba}_3\text{Sc}_{1.9}\text{Al}_{0.1}\text{B}_4\text{O}_{12}:\text{Eu}^{2+}$  Excited by NUV Light. *Opt. Mater.* **2019**, 92, 195-205.

(19) Wei, Y.; Gao, Z.; Liu, S.; Chen, S.; Xing, G.; Wang, W.; Dang, P.; Li, G., Highly Efficient Green - to - Yellowish - Orange Emitting  $\text{Eu}^{2+}$  - Doped Pyrophosphate Phosphors with Superior Thermal Quenching Resistance for w - LEDs. *Adv. Opt. Mater.* **2020**, 8, 1901859.

(20) Aggarwal, R.; Ranganathan, P., Common Pitfalls in Statistical Analysis: Linear Regression Analysis. *Perspect Clin. Res.* **2017**, 8, 100-102.

(21) Antoni J. Duleba.; David L. O., Regression Analysis and Multivariate Analysis. *Sem. Reprod. Med.* **1996**, 14, 139-153.

(22) Qiao, J.; Amachraa, M.; Molokeyev, M.S.; Chuang, Y.; Ong, S.; Zhang, Q.; Xia, Z., Engineering of  $\text{K}_3\text{YSi}_2\text{O}_7$  To Tune Photoluminescence with Selected Activators and Site Occupancy. *Chem. Mater.* **2019**, 31, 7770-7778.

(23) Qiao, J.; Zhou, G.; Zhou, Y.; Zhang, Q.; Xia, Z., Divalent Europium-Doped Near-Infrared-Emitting Phosphor for Light-Emitting Diodes. *Nat. Commun.* **2019**, 10, 5267.

(24) Qiao, J.; Ning, L.; Molokeyev, M.S.; Chuang, Y.; Zhang, Q.; Kenneth R. Poeppelmeier.; Xia, Z., Site-Selective Occupancy of  $\text{Eu}^{2+}$  Toward Blue-Light-Excited Red Emission in a  $\text{Rb}_3\text{YSi}_2\text{O}_7:\text{Eu}$  Phosphor. *Angew. Chem.* **2019**, 131, 11645-11650.

(25) Vidican, I.; Smith, M. D.; zur Loye, H. C., Crystal Growth, Structure Determination, and Optical Properties of New Potassium-Rare-Earth Silicates  $\text{K}_3\text{RESi}_2\text{O}_7$  (RE= Gd, Tb, Dy, Ho, Er, Tm, Yb, Lu). *J. Solid State Chem.* **2003**, 170, 203-210.

(26) Dang, P.; Li, G.; Liang, S.; Lian, H.; Lin, J., Multichannel Photoluminescence Tuning in Eu-Doped Apatite Phosphors via Coexisting Cation Substitution, Energy Transfer and Valence Mixing. *J. Mater. Chem. C.* **2019**, 7, 5975-5987.

(27) Liu, Y.; Zhang, J.; Zhang, C.; Xu, J.; Liu, G.; Jiang, J.; Jiang J.,  $\text{Ba}_9\text{Lu}_2\text{Si}_6\text{O}_{24}:\text{Ce}^{3+}$ : An Efficient Green Phosphor

with High Thermal and Radiation Stability for Solid-State Lighting. *Adv. Opt. Mater.* **2015**, 3, 1096.

(28) Wang, S.; Song, Z.; Kong, Y.; Liu, Q. Relationship of Stokes Shift with Composition and Structure in  $\text{Ce}^{3+}/\text{Eu}^{2+}$ -doped Inorganic Compounds. *J. Lumin.* **2019**, 212, 250-263.

(29) Qiu, Z.; Lian, H.; Shang, M.; Lian, S.; Lin, J., The Structural Evolution and Spectral Blue Shift of Solid Solution Phosphors  $\text{Sr}_{3-m}\text{Ca}_m\text{B}_2\text{O}_6:\text{Eu}^{2+}$ . *Cryst. Eng. Comm.* **2016**, 18, 4597-603.

(30) Ji, H.; Wang, L.; Molokeyev, M.; Hirosaki, N.; Xie, R.; Huang, Z.; Xia, Z.; Kate, O.; Liu, L.; Atuchin, V., Structure Evolution and Photoluminescence of  $\text{Lu}_3(\text{Al},\text{Mg})_2(\text{Al},\text{Si})_3\text{O}_{12}:\text{Ce}^{3+}$  Phosphors: New Yellow-Color Converters for Blue LED-Driven Solid State Lighting. *J. Mater. Chem. C.* **2016**, 4, 6855-63.

(31) Daicho, H.; Shinomiya, Y.; Enomoto, K.; Nakano, A.; Sawa, H.; Matsuishi, S.; Hosono, H. A Novel Red-Emitting  $\text{K}_2\text{Ca}(\text{PO}_4)\text{F}:\text{Eu}^{2+}$  Phosphor with A Large Stokes Shift. *Chem. Commun.* **2018**, 54, 884-887.